International Journal of Nanomedicine

Dovepress
open access to scientific and medical research

Open Access Full Text Article

ORIGINAL RESEARCH

Magnetic-luminescent $YbPO_4$:Er,Dy microspheres designed for tumor theranostics with synergistic effect of photodynamic therapy and chemotherapy

This article was published in the following Dove Press journal:
International Journal of Nanomedicine
20 October 2014
Number of times this article has been viewed

Wei Wang
Dong Xu
Xiaojun Wei
Kezheng Chen

[1]Lab of Functional and Biomedical Nanomaterials, College of Materials Science and Engineering, Qingdao University of Science and Technology, Qingdao, People's Republic of China

Abstract: In this paper, magnetic and fluorescent bifunctional $YbPO_4$:Er,Dy microspheres were synthesized via a simple solvothermal method. The prepared microspheres exposed to 980 nm near-infrared (NIR) laser light emitted bright upconversion fluorescence (450–570 nm) after calcination at high temperatures (>800°C). Results of magnetic resonance studies demonstrated that the $YbPO_4$:Er,Dy microspheres are more suitable to be used as a transverse relaxation time (negative) contrast magnetic resonance imaging agent. The microspheres successfully entered the human hepatocellular carcinoma cells and presented low toxicity. A well-selected photodynamic therapy (PDT) drug, merocyanine 540 (MC540) with an ultraviolet–visible spectroscopy absorption maximum of 540 nm, was loaded onto the microspheres to obtain $YbPO_4$:Er,Dy-MC540. Since the upconversion fluorescence emitting from the microspheres could be absorbed by MC540 with a small absorption/emission disparity, $YbPO_4$:Er,Dy-MC540 could kill the hepatocellular carcinoma cells via PDT mechanism effectively. In other words, being upconverting particles, the prepared microspheres acted as light transducers in the NIR light-triggered PDT process. A chemotherapy drug, doxorubicin, was further loaded onto $YbPO_4$:Er,Dy-MC540 to achieve enhanced antitumor effect based on synergistic therapeutic efficacy of PDT and chemotherapy. It is expected that the prepared $YbPO_4$:Er,Dy microspheres have applications in tumor theranostics including magnetic-fluorescent bimodal imaging and NIR light-triggered PDT.

Keywords: fluorescent, lanthanide, upconversion

Introduction

Over the past few decades, there have been many reports on the application of magnetic-fluorescent nanomaterials in biological labeling/imaging. Conventional organic fluorophores and semiconductor quantum dots always suffer from several disadvantages, including high background noise and considerable photodamage to biological materials associated with ultraviolet (UV) excitation, low photobleaching threshold, and potential long-term toxicity.[1–5] Therefore, it is highly desirable to develop new-generation bioprobes to circumvent the above limitations of traditional ones. Upconversion nanocrystals (UCNPs) converting near-infrared (NIR) excitation into a visible emission through lanthanide doping have emerged as promising candidates in the field of biophotonics and biomedical imaging. They offer high photo- and chemical stability, sharp emissions, and large anti-Stokes shifts when compared to the conventional luminescent materials.[6] Due to the electronic transitions of rare-earth (RE) ions between the 4f energy level, RE compounds are regarded as potential laser host materials, oxygen ion conductors, and fluorescent lamp phosphors. Moreover, they

Correspondence: Wei Wang
No 53 Zhengzhou Road, Qingdao, People's Republic of China, 266042
Tel +86 532 8402 2814
Fax +86 532 8402 2814
Email wangwei@qust.edu.cn

are superior to downconversion materials in that they: have deeper light penetration depth without tissue autofluorescence; have an absence of photobleaching and photoblinking; and cause less harm to biological specimens.[3–5,7] The reported matrix material examples include $NaYF_4$ nanocrystals,[8–10] zinc sulfide nanoparticles,[11] zinc oxide nanoparticles,[12,13] lanthanide oxides,[14,15] and so on. Phosphate compounds are also an appropriate matrix for RE ions because they are stable at high temperatures and hence can overcome the drawbacks of poor thermal stability and mechanical properties of other RE compounds.[16–18] RE phosphates have been considered as good candidates for phosphors, catalyst, biological detection, and so on.[19,20] Furthermore, varying the trivalent lanthanide ions (Ln^{3+}) concentration or introducing two or more types of Ln^{3+} ions into a suitable host changes the luminescence properties of these materials. In upconversion materials, Yb^{3+} is the most widely employed sensitizer because of its high absorption cross-section at ~980 nm. It may efficiently transfer the absorbed photons to the emitting Ln^{3+} energy level, resulting in a light emission ranging from the UV to NIR that may be employed in various industrial applications.[6,21,22]

Magnetic resonance imaging (MRI) is one of the most powerful bioimaging techniques in tumor theranostics, because it provides precise anatomical information with deep penetration into tissue in a noninvasive manner.[23,24] Fluorescence imaging is also one of the most significant applications of luminescent nanoparticles in bioanalysis for detection and sensing. Many studies have shown that the use of MRI and fluorescence imaging are complementary to each other in the aspect of spatial resolution and depth perception. For this reason, efforts have been devoted to synthesize and investigate materials which are fluorescent–magnetic bimodal.[11]

Photodynamic therapy (PDT) is a treatment of cancer performed in a noninvasive mode and involves the use of light with specific wavelength and PDT drugs called photosensitizers (PS). The mechanism of PDT is based on the photochemical reactions between surrounding oxygen and PS. When exposed to a specific light, PS produces cytotoxic reactive oxygen species (ROS) which can induce apoptosis of cancer cells. Being a minimally invasive therapeutic modality, PDT has gained increasing interest in biotechnology. However, some drawbacks, including limited penetration depth of the specific light and poor water solubility of PS, greatly limited the clinical development of PDT.[25,26] NIR light-triggered PDT that utilizes specific light with excitation wavelength in the NIR region can overcome the drawbacks of traditional PDT because the NIR region is a light-transparent window in the tissue due to less absorption and less scattering than visible light, and hence has deeper penetration than visible light. Moreover NIR light can effectively reduce the photosensitivity of PS to ambient light.[27–30] However, most of the photochemical reactions of available PS can only be activated by visible light rather than NIR light. UCNPs therefore are anticipated to act as nanotransducers to solve the problems that traditional PDT has faced, since they can convert NIR light to visible light which is necessary to activate the photochemical reactions of PS.

It is believed that PS drugs combined with the UCNPs can further enhance the efficiency of PDT treatment because the small size of nanoparticles favors the delivery and excretion of the PS as a PDT drug. As a result, many types of UCNP/PS-based PDT drugs have been developed in the past few years.[31–33] The first report on UCNP-triggered PDT was performed by Zhang et al in the year 2007.[32] The UCNPs used in this study are $NaYF_4$:Yb^{3+},Er^{3+} photo upconverting nanoparticles, which were coated by a porous silica shell. Merocyanine 540 (MC540) with the maximum absorption at 540 nm was used as PS drug, and encapsulated into the silica layer during the coating process. In vitro PDT tests were performed to confirm the PDT cytotoxicity of the MC540-coated UCNPs toward MCF-7/AZ breast cancer cells. In order to bring the UCNPs close enough to the target cancer cells, a mouse monoclonal antibody, anti-MUC1/episialin, was covalently attached to the UCNPs based on the antigen–antibody interaction with good specificity. Fluorescent property studies showed that the UCNPs excited by 974 nm infrared source could emit strong upconverting light with wavelengths of 537 and 635 nm. The upconverting light was then absorbed by MC540 and generated ROS to kill the MCF-7/AZ breast cancer cells.

Other examples on the application of UCNP/PS composite nanomaterials for PDT include zinc phthalocyanin (ZnPc)-folic acid-poly(ethylene imine) /$NaYF_4$:Yb^{3+},Er^{3+} nanoparticles,[33] NaY(Mn)F_4:Yb,Er nanocrystals coated by doublelayered Chlorin e6,[34] $NaYF_4$:Yb^{3+},Er^{3+} nanocrystals coated by *meso* -tetraphenyl porphine,[30] $LiYF_4$:Yb/Er coupled with β-carboxyphthalocyanine zinc,[35] $NaYF_4$:Yb,Er/$NaGdF_4$-Chlorin e6 core-shell nanoparticles,[36] $NaGdF_4$:Yb,Er@CaF_2@SiO_2 nano-phosphors covalently grafted to hematoporphyrin and silicon phthalocyanine dihydroxide,[37] tetra-sulfonic phthalocyanine aluminium photosensitizers conjugated Fe_3O_4@$NaYF_4$:Yb/Er,[38] $NaYF_4$:Er,Yb@SiO_2-ZnPc nanoparticles,[39,40] ZnO:Er,Yb,Gd-methylene blue,[15] and so on.

In this study, we systematically investigated novel $YbPO_4$:Er,Dy microspheres including their preparation, morphology, structure, fluorescent/magnetic properties, and bioapplications in tumor theranostics. Under NIR excitation, the prepared microspheres can emit green-colored upconversion

fluorescence which can be absorbed by MC540 loaded onto the microspheres and kill tumor cells via PDT mechanism. In order to achieve enhanced antitumor effect based on synergistic therapeutic efficacy of PDT and chemotherapy, a chemotherapy drug termed doxorubicin (DOX) was loaded onto the $YbPO_4$:Er,Dy microspheres.

Material and methods

Material

All reagents used were of analytical quality. For the synthesis, the following reagents were used: Yb_2O_3; Er_2O_3 and Dy_2O_3 (analytical reagent); nitric acid (HNO_3, 65.0%–68.0%); ammonium phosphate monobasic $(NH_4)_2HPO_4$ (analytical reagent); ethylene glycol; and glycero (99.0%) from Sinopharm Chemical Reagent Co., Ltd., China (Mainland). The water used in this study was deionized by a Milli-Q Plus system, whose electrical resistance was 18.2 MΩ.

For cell culture experiments, the following reagents were used: Roswell Park Memorial Institute (RPMI)-1640 medium and fetal bovine serum (FBS) from HyClone, Thermo Scientific, Logan, Utah, USA; methyl thiazolyl tetrazolium (MTT); trypan blue (TB); dimethyl sulfoxide; MC540; and DOX from Sigma-Aldrich Co., (St Louis, MO, USA). The medium was supplemented by antibiotics to inhibit bacterial growth. Penicillin and streptomycin were used in combination. The final concentration of the penicillin or streptomycin was 100 units per mL. When used, 1 mL glutamine solution (0.2 M) was further added to 100 mL culture medium.

Synthesis of $YbPO_4$:Er,Dy microspheres

RE oxides dissolved by nitric acid in 80°C water bath conditions and $(NH_4)_2HPO_4$ dissolved by deionized water were evenly blended. The solution was added to polyol solvent mixture of glycol and glycerol, and then heated at 180°C for 12 hours. The as-prepared products were washed with ethanol and deionized water several times, centrifuged at 8,000 rpm, dried for 24 hours at 80°C in the air, and annealed at high temperatures (600°C–1,200°C) for 2 hours.

Characteristics of $YbPO_4$:Er,Dy microspheres

The X-ray diffraction (XRD) patterns were obtained with a RIGAKU, Tokyo, Japan D/MAR-2500 powder X-ray diffraction in the 2θ range from 10° to 80°. The reference data were taken from the ICSD (Inorganic Crystal Structure Database). Scanning electron microscope (SEM) and Energy-dispersive X-ray spectroscopy (EDS) characterization were performed by a JEOL Ltd., Tokyo, Japan JSM-6700F field emission SEM.

Fluorescence measurement was carried out at room temperature with F-4600 fluorescence spectrometer (Hitachi Ltd., Tokyo, Japan). Excitation and emission spectra were corrected for instrumental response. For the upconversion measurements, the solid-state 980 nm laser was used as the excitation source. Magnetic properties were performed using a 1.5 T MRI system (Bruker, Billerica, Massachusetts, Germany mq60 NMR analyzer) at 300 K. Ultraviolet–visible–NIR spectrophotometer (Cary500; Varian Inc., Palo Alto, California, USA) was used to investigate the loading of MC540 and DOX onto the $YbPO_4$:Er,Dy microspheres.

Preparation of $YbPO_4$:Er,Dy-MC540 and $YbPO_4$:Er,Dy-MC540-DOX microspheres

MC540 was selected as the photosensitizer. MC540 loading onto the $YbPO_4$:Er,Dy microspheres was carried out by mixing MC540 (20 μM) with $YbPO_4$:Er,Dy microspheres (0.2 mg/mL) in phosphate-buffered saline (PBS) and stirring at room temperature for 12 hours. MC540-loaded samples ($YbPO_4$:Er,Dy-MC540) were separated from the free-standing MC540 molecules through centrifugation at 8,000 rpm for 5 minutes and carefully washed three times with PBS. The formed $YbPO_4$:Er,Dy-MC540 samples were resuspended in PBS and stored at 4°C. MC540 concentration in supernatant was analyzed by the ultraviolet–visible absorption at the wavelength of 540 nm (A_{540}) with reference to a calibration curve (Figure S1A) which was obtained by measuring A_{540} of a set of standard MC540 samples of known concentrations. The measurements were performed in triplicate. The amount of MC540 in $YbPO_4$:Er,Dy-MC540 could be determined by subtracting MC540 amount in supernatant from the initial amount of MC540 mixed with $YbPO_4$:Er,Dy microspheres. The loading procedure of DOX was carried out using a similar method, and the loading amount of DOX was determined with the help of the calibration curve (Figure S1B) which plots the relationship between A_{480} and DOX concentration.

Biocompatibility assessment of $YbPO_4$:Er,Dy microspheres

The human hepatocellular carcinoma cancer cell line (HepG2 cells) was originally obtained from the China Center of Type Culture Collection, Wuhan, China and cultured in RPMI-1640 with 10% FBS, 1% dual-antibiotic (the final concentration of the penicillin or streptomycin is 100 units per mL), and 2 mM glutamine.

MTT viability assay, a colorimetric measure of mitochondrial activity, was used to assess the biocompatibility of the nanospheres. HepG2 cells were cultured in a 96-well plate (Costar; approximately 5×10^3 cells per well) with 1,640 medium

containing 10% FBS and different concentrations of the $YbPO_4$:Er,Dy microspheres for different times. After 24 hours' incubation with the prepared microspheres with 5% CO_2 in the medium at 37°C, the supernatant of each well was removed and washed twice with PBS. Then, 20 μL of MTT solution (5 mg/mL MTT in PBS) was added to each well and the mixtures incubated for 4 hours at 37°C. Then, the medium was removed and the absorbance of each well at 490 nm was measured on a microplate reader as a blank value, OD_{blank}. After removing the medium, intracellular formazan crystals were extracted into 150 μL of dimethyl sulfoxide and quantified by measuring the absorbance of the cell lysate at 490 nm as a sample value OD_{sample}. Cell viability was calculated by Equation 1:

$$\text{Cell viability} = \frac{OD_{sample} - OD_{blank}}{OD_{control}} \times 100\% \quad (1)$$

where $OD_{control}$ is the absorbance of negative control value (cells incubated without samples). All experiments were repeated four times and the resulting data were processed with statistical methods.

Cell uptake of $YbPO_4$:Er,Dy microspheres

HepG2 cells were seeded in a 6-well plate (Costar) with a density of 1×10^4 cells/well and cultured in RPMI-1640 medium supplemented with 10% FBS, 1% dual-antibiotic, and 2 mM glutamine. After 24 hours of incubation in the incubator (37°C, 5% CO_2), each well was washed with sterile PBS, followed by addition of RPMI-1640 medium containing $YbPO_4$:Er,Dy microspheres with concentration of 0.1 mg/mL. The cells were further incubated for 24 hours and the medium was removed. Then the cells were washed with PBS three times and fixed by 4% paraformaldehyde/PBS for 1 hour at room temperature for confocal laser microscope (FLUO View TMFV 1000; Olympus Corporation, Tokyo, Japan) analysis. The optical-section images at different depths were obtained by changing the focal plane of the confocal laser scanning microscope (CLSM). The removed media was collected and centrifuged at 8,000 rpm for 10 minutes to extract remnant microspheres not swallowed by cells. The mass of remnant microspheres was obtained after being washed with deionized water and dried for 24 hours at 80°C in the air.

Antitumor effect of $YbPO_4$:Er,Dy-MC540 and $YbPO_4$:Er,Dy-MC540-DOX microspheres

$YbPO_4$:Er,Dy samples with different MC540 or DOX loading amounts were first sterilized with a disinfection boiler and dispersed in culture medium. HepG2 cells were incubated in the incubator (37°C, 5% CO_2) with $YbPO_4$:Er,Dy dispersed in RPMI-1640 medium with different $YbPO_4$:Er,Dy concentrations of 125–1,000 μg/mL. Then, the cells were washed several times with PBS. After 12 hours' incubation, $YbPO_4$:Er,Dy samples were removed and the cells were washed twice with PBS. After that, the cells were irradiated by 980 nm laser light (0.5 W) for 3 minutes. To avoid a possible overheating effect caused by the 980 nm light in the long period of radiation, the laser was switched on for 1 minute at a time, with 1 minute of darkness between each instance. Cell viabilities were assessed by MTT method after incubation for an additional 12 hours. Finally, the cells were washed with PBS and stained with 0.4% TB. Microscopy images of cells were obtained with an inverted microscope (Eclipse TE2000S; Nikon Corporation, Tokyo, Japan).

Statistical analysis

Data were analyzed using Excel 2003 software. Statistical significance was determined by Student's *t*-test. Differences were considered significant where $P<0.05$.

Results and discussion

Structure and morphology of $YbPO_4$:Er,Dy microspheres

Figure 1 shows the XRD patterns of $YbPO_4$:Er,Dy microspheres sintered at different temperatures. The peaks centered at 19.746°C, 26.117°C, 32.956°C, 37.269°C, 35.328°C, 42.529°C, and 52.292°C respectively correspond to $YbPO_4$ (101), (200), (211), (112), (220), (301), and (312) crystal faces (JCPDS#45-0530). As the sintering temperature increases, the peaks become narrower and more acute, indicating improved crystallinity of the samples as well

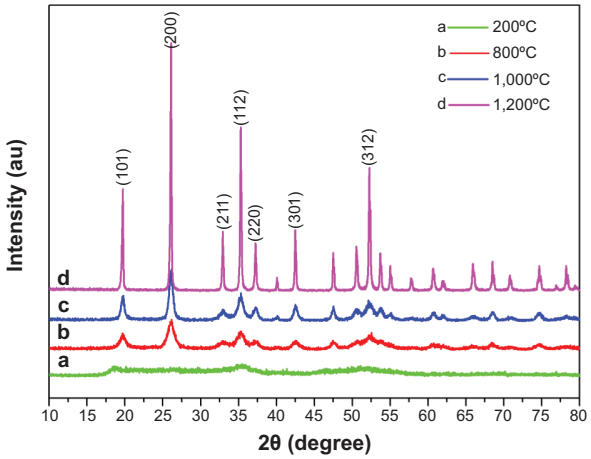

Figure 1 XRD patterns of $YbPO_4$:Er,Dy microspheres.
Abbreviation: XRD, X-ray diffraction.

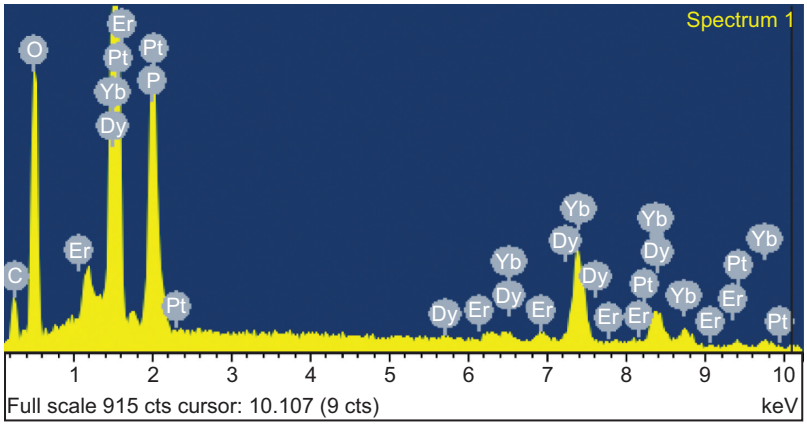

Figure 2 The EDS pattern of $YbPO_4$:Er,Dy microspheres sintered at 800°C.
Abbreviations: cts, counts; EDS, Energy-dispersive X-ray spectroscopy.

as increased crystal size. EDS was employed to further analyze the composition of the $YbPO_4$:Er,Dy microspheres (Figure 2), which revealed that the as-synthesized products were composed of Yb, Er, P, Dy, and O elements. The Si signal may come from the silicon wafer to support the $YbPO_4$:Er,Dy sample, and the Pt signal may be a result of Pt deposition onto the $YbPO_4$:Er,Dy to obtain SEM images with high quality. The C signal may be generated not only by alcohol used to disperse the $YbPO_4$:Er,Dy sample for SEM characterization, but also by the carbon impurity produced in the post-thermal treatment in air.

SEM image (Figure 3A) and dynamic light scattering (DLS) chart (Figure 3B) show spherical morphology of the prepared particles with an average diameter of 1,308.22 nm. The solvent greatly influenced the size distribution of the products. Mixed solvent of ethylene glycol and glycerol with a volume ratio of 1:3, respectively, favors the formation of uniform $YbPO_4$:Er,Dy microspheres with a polydispersity index of 0.236, demonstrating a narrow size distribution of the prepared microspheres.

Compared with the products desiccated at 200°C (Figure S2A), the particle size, distribution, and morphology did not change greatly after sintering at 800°C for 1.5 hours (Figure S2B). The surface of the spheres became smoother, which may be due to improved crystallinity of the spheres. The products sintered at 1,200°C for 1.5 hours (Figure S2C) exhibited a much different morphology, indicating that recrystallization might occur during the annealing process at 1,200°C.

Magnetic resonance properties of $YbPO_4$:Er,Dy microspheres

Dysprosium (Dy) compounds are known to be able to serve as transverse relaxation agents[41,42] through accelerating transverse relaxation time (T_2) of water protons and exerting dark contrast in regions where the compounds localize. To evaluate their effectiveness as MRI agents, the T_2

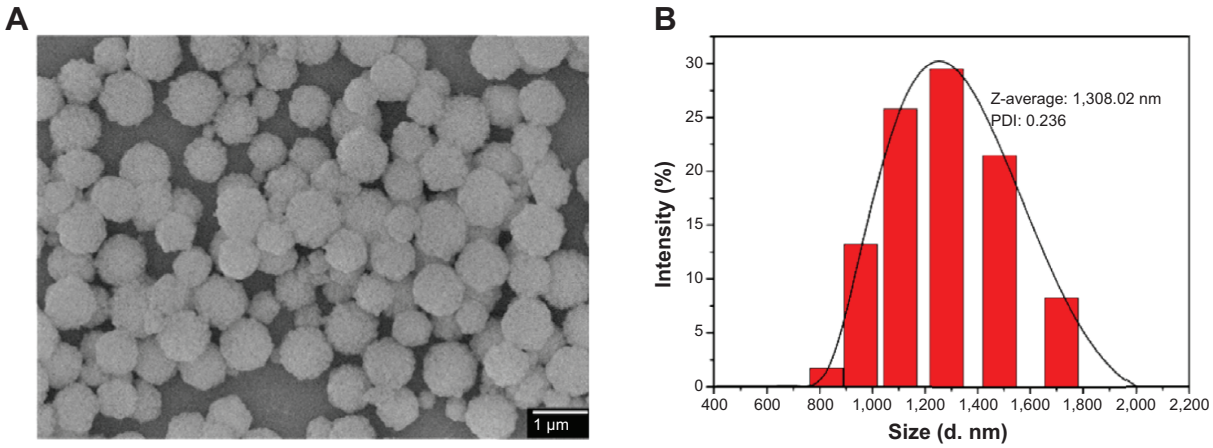

Figure 3 SEM image and DLS of $YbPO_4$:Er,Dy microspheres sintered at 800°C.
Notes: (**A**) SEM image. (**B**) DLS.
Abbreviations: DLS, dynamic light scattering; PDI, polydispersity index; SEM, scanning electron microscope.

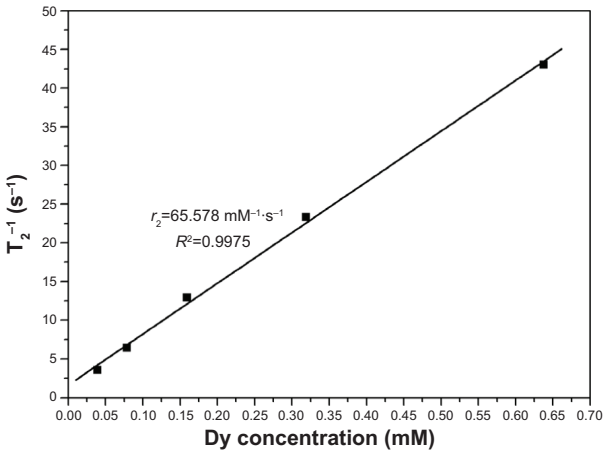

Figure 4 The linear relationship between transverse relaxation rates and Dy ion concentrations for $YbPO_4$:Er,Dy microspheres.
Abbreviations: r_2, nuclear transverse relaxivity; T_2, transverse relaxation time.

of the $YbPO_4$:Er,Dy aqueous suspensions was examined using a 1.5 T MRI system with clinical field strength at physiological temperature (37°C). Figure 4 plots the linear relationship between the transverse relaxation rate ($1/T_2$) and Dy concentration, and the slope of the plot was determined to be the nuclear transverse relaxivity with a value of 65.578 $mM^{-1}·s^{-1}$, which represents the efficiency of the magnetic material as a T_2 contrast agent.

Upconversion luminescence of $YbPO_4$:Er,Dy microspheres

Figure 5A shows upconversion fluorescent spectra of $YbPO_4$:Er,Dy samples sintered at different temperatures and characterized by using a fluorescence spectrometer (photomultiplier tube voltage of 700 V, excitation wavelength of 980 nm). We found that $YbPO_4$:Er,Dy samples sintered at the temperatures below 800°C showed no significant upconversion fluorescence which may be due to their poor crystallinity, carbon impurities, and residual water or OH groups. Whereas for the samples sintered at the temperatures higher than 1,000°C, the fresh green-light emissions between 500 and 570 nm were observed to $^2H_{11/2}\rightarrow{}^4I_{15/2}$ and $^4S_{3/2}\rightarrow{}^4I_{15/2}$ conversion of Er^{3+}, while weak red emissions between 630 and 690 nm were observed to $^4F_{9/2}\rightarrow{}^4I_{15/2}$ conversion.[43,44] With the increasing of sintering temperature from 800°C to 1,200°C, the emission intensity increases due to improved crystallinity of the microspheres, homogeneous distribution of Er^{3+} ions, and absence of carbon impurities and residual water or OH groups. Figure 5B shows that for all samples with different lanthanide doping content, the green-light emission is much stronger than the red light. Although the samples doped with Dy^{3+} have been proven to present excellent magnetic behavior, the introduction of Dy^{3+} greatly suppressed the upconversion fluorescence of $YbPO_4$:Er,Dy (Figure 5B). In order to obtain an optimized fluorescent–magnetic bifunctionality, we choose the Yb:Er:Dy =100:5:5 sample sintered at 1,200°C for further experiments including in vitro biocompatibility assessment and PDT test.

The upconversion mechanism was studied by investigating the relationship between the upconversion emission intensity (I_{up}) and excitation power (P). Figure 6A demonstrates the dependence of I_{up} on P of our $YbPO_4$:Er,Dy powder samples. The line of log (I_{up}) versus log(P^N) shown in Figure 6B is fitted according to the well-known Equation 2:[44]

$$I_{up} \propto P^N \Rightarrow log(I_{up}) = \log(kP^N) = NlogP + A \qquad (2)$$

where N is the number of photons required to produce one upconversion emission photon and determined by the slope of the fitted line. In our study, all the N values were calculated to be approximately 2, indicating two-photon process for the upconversion emission.

To better understand the observed Yb^{3+} to Er^{3+} energy-transfer mechanism, a schematic representation similar to our reported results of the partial energy-level diagram and the possible energy-transfer pathways is presented in Figure S3. Typically, one Yb^{3+} ion absorbs energy of a 980 nm photon from the excitation light. The energy is transferred from the $^2F_{5/2}$ level of Yb^{3+} ion to the ground state of Er^{3+} ion. Then the $^4I_{15/2}\rightarrow{}^4I_{11/2}$ transition of Er^{3+} occurs accompanied by $^4I_{13/2}$ level generation of Er^{3+} through multiphonon relaxation process. After that, Er^{3+} ions transfer to higher levels ($^4F_{7/2}$ and $^4F_{9/2}$ levels) as a result of two energy transformations from $^2F_{5/2}$ of Yb^{3+} to the $^4I_{13/2}$ and $^4I_{9/2}$ levels of Er^{3+}. The $^4S_{3/2}/^2H_{11/2}$ and $^4F_{9/2}$ levels are subsequently generated by multiphonon relaxation. Lastly, green and red emissions are obtained with the electronic transitions of $^4S_{3/2}/^2H_{11/2}\rightarrow{}^4I_{15/2}$ and $^4F_{9/2}\rightarrow{}^4I_{15/2}$ of Er^{3+}, respectively.[44,45]

Biocompatibility assessment of $YbPO_4$:Er,Dy microspheres

Generally, the actual biological application of samples needs to address the question about its biocompatibility. Low or no cytotoxicity is one of the most critical parameters for ideal biomaterials. To evaluate the cytotoxicity of the as-prepared sample, we used the MTT assay method to measure the relative cell viability. This method was widely used to measure the mitochondria activity to quantify cell death. The final results were expressed as the average of four parallel experiments ± the standard deviations (denoted as error

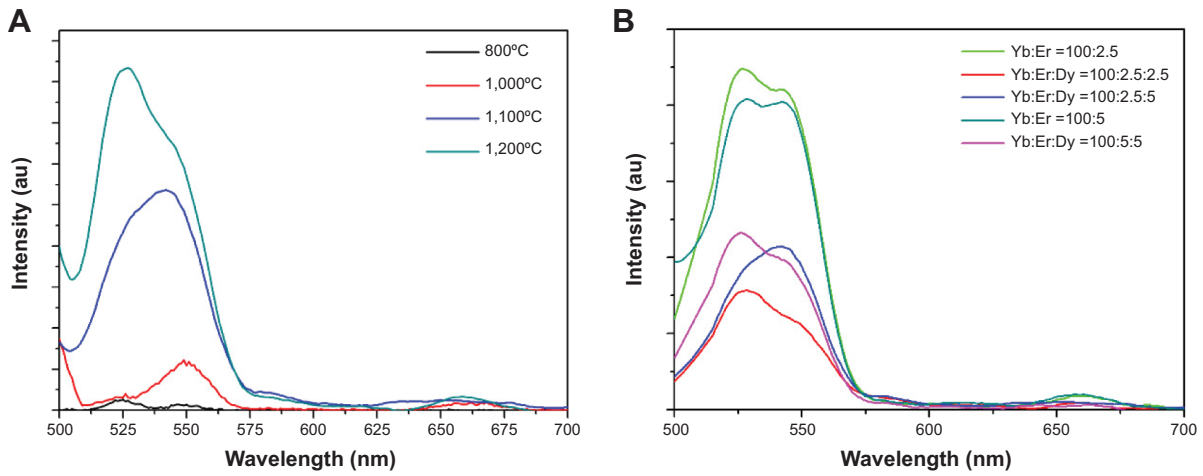

Figure 5 Fluorescence spectra of $YbPO_4$:Er,Dy samples.
Notes: The fluorescence spectra of $YbPO_4$:Er,Dy samples (**A**) annealed at different temperatures (Yb:Er:Dy =100:2.5:5 for all samples, λ_{EX}=980 nm) (**B**) with different doping ratio (annealed at 1,200°C, λ_{EX}=980 nm).

bars in Figure 7) of cell viability. The "1" columns shown in Figure 7 demonstrated that a desirable cell viability of 95.15%±5.01% was obtained even at high concentration of ~1,000 μg/mL $YbPO_4$:Er,Dy microspheres. The viabilities were 96.77%±4.45%, 97.47%±7.22%, and 99.32%±3.65% at concentrations of 500, 250, and 125 μg/mL, respectively, and not significantly different from the untreated control (100%). These data suggest that incubation in the presence of the $YbPO_4$:Er,Dy microspheres did not significantly affect the cell viability, indicating favorable biocompatibility of the microspheres.

A region of HepG2 cells was observed by the CLSM microscope, which can handle living cells without causing damage to the physical and chemical properties of the cell. In the CLSM images shown in Figure 8, plenty of black spots were observed inside cell cytoplasm which cannot be seen in untreated cells (data not shown). Since CLSM images are optical-section images able to display three-dimensional structure of the cells, it can be concluded that the $YbPO_4$:Er,Dy microspheres were internalized into cells and located in cell cytoplasm. It is noticed that HepG2 cells maintained a fine spindle shape because the cell still adhered on the substrate even after internalization of the microspheres. Cell membrane also appeared clear-edged, further indicating the desirable biocompatibility of our products.

Many cell types have been reported to actively ingest microscale particles and the ideal size of microspheres for this purpose ranges from about 0.5 to 2 μm.[46–48] The particles

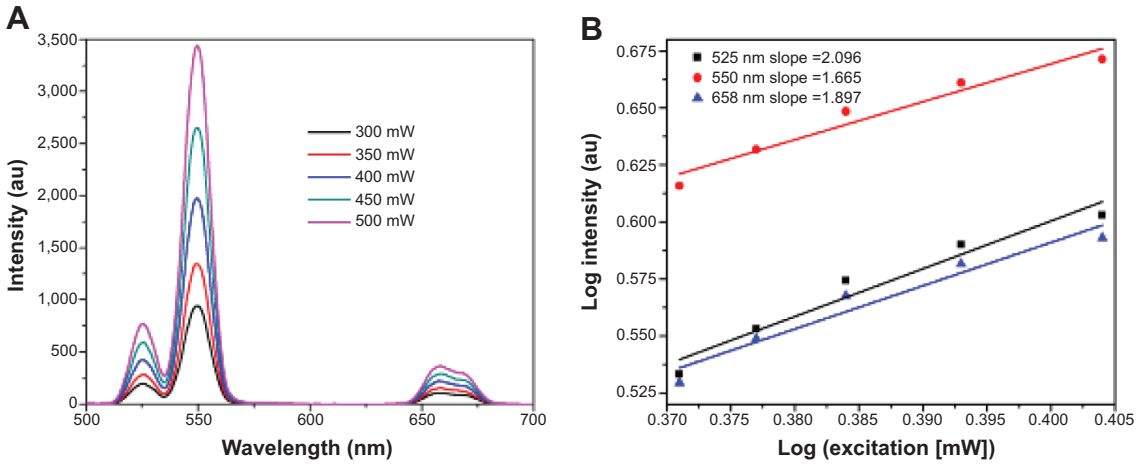

Figure 6 The relationship between the upconversion emission intensity (I_{up}) and excitation power (P) of $YbPO_4$:Er.
Notes: (**A**) The fluorescence spectra of $YbPO_4$:Er annealed at 1,100°C excited with a 980 nm near-infrared laser at different pump powers. (**B**) The corresponding plots (log–log) of emission intensity versus pump power of $YbPO_4$:Er annealed at 1,100°C.

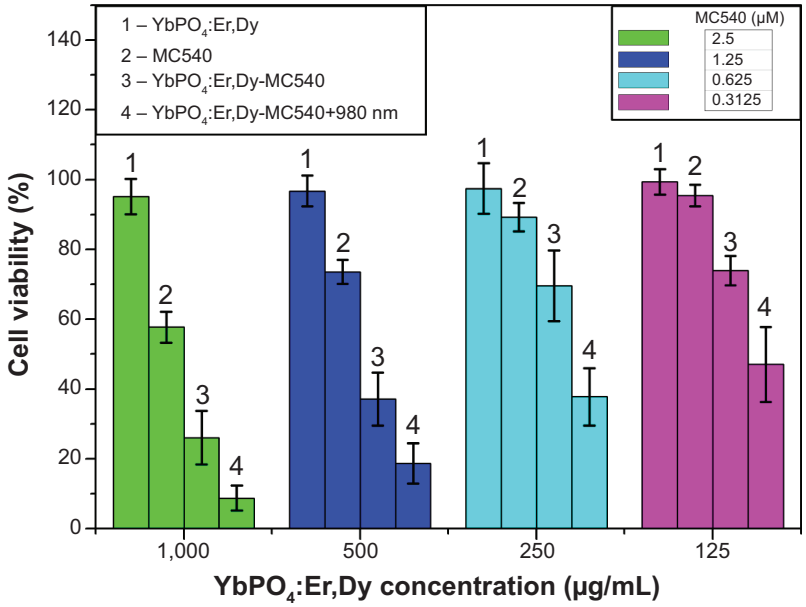

Figure 7 Cell viability data of HepG2 cells showing the PDT effect of $YbPO_4$:Er,Dy-MC540.
Notes: Data presented as mean ± standard deviation (n=4). $P<0.05$ when compared with control.
Abbreviations: HepG2, hepatocellular carcinoma cancer cell line; MC540, merocyanine 540; PDT, photodynamic therapy.

can enter cells through different ways including phagocytosis, fluid-phase, endocytosis, and receptor-mediated endocytosis. The main way is endocytosis although these ways have been shown to be performed simultaneously.[13] This is true of our $YbPO_4$:Er,Dy microspheres which may be promoted by the transferrin component of FBS used in our study during incubation of $YbPO_4$:Er,Dy with HepG2 cells.

The uptaking efficiency of $YbPO_4$:Er,Dy microspheres was calculated to be 31.91% by Equation 3:

$$\text{Uptaking efficiency} = \frac{m_1 - m_2}{m_1} \times 100\%, \qquad (3)$$

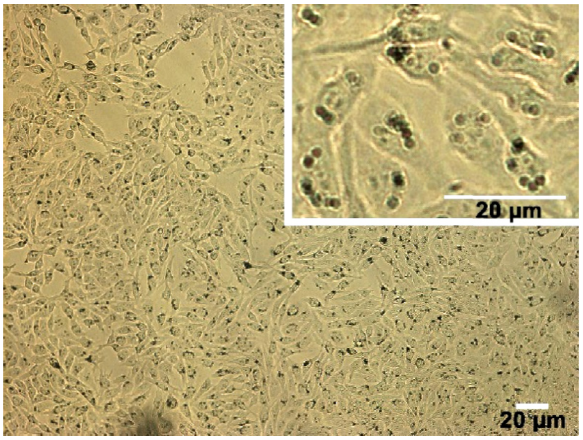

Figure 8 Confocal laser scanning microscopic images of hepatocellular carcinoma cancer cells incubated with $YbPO_4$:Er,Dy microspheres.

where m_1 is the mass of $YbPO_4$:Er,Dy microspheres added in the incubation medium and m_2 is the mass of remnant microspheres after incubation with HepG2 cells for 24 hours.

Photodynamic therapy and chemotherapy of HepG2 cells

Excellent upconversion fluorescent properties, successful cell uptake, and low toxicity provide the premise for the prepared $YbPO_4$:Er,Dy spheres to serve as light transducers in further PDT-related experiments.

As mentioned above, PDT is based on apoptosis of cancer cells induced by ROS generated from the photochemical reactions between surrounding oxygen and PS excited by specific light.[33] For NIR-triggered PDT, PS absorb visible light emitting from the upconverting materials and then are excited to higher energy-level states. In order to acquire high ROS-generation efficiencies, the wavelength disparity between PS absorption and upconverting materials emission should be as small as possible. As a result, MC540 that absorbs light just within the range of our $YbPO_4$:Er,Dy emission band, ie, 450–570 nm, was selected as the PDT drug. Figure 9A confirms the small disparity between MC540 absorption and $YbPO_4$:Er,Dy emission within the green-light-band range, and the antitumor mechanism of our $YbPO_4$:Er,Dy-based PDT drug is schematically illustrated in Figure 9B.

Based on the results, $YbPO_4$:Er,Dy-MC540 was developed as a PDT drug in our study by loading MC540 onto $YbPO_4$:Er,Dy

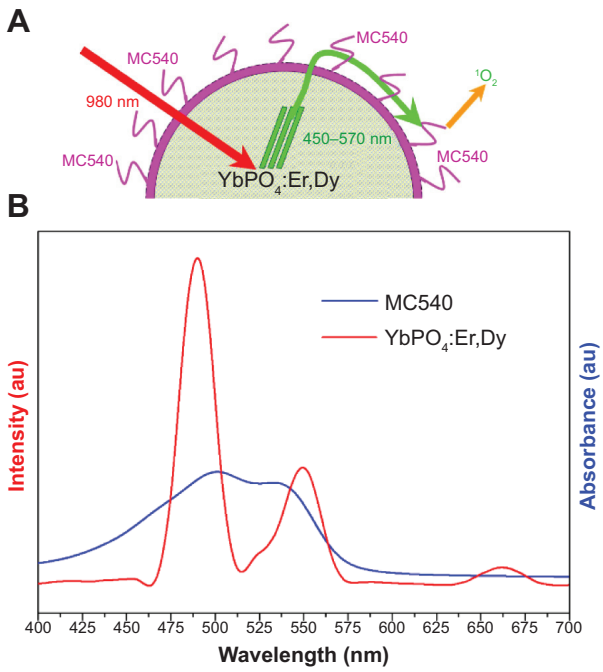

Figure 9 Mechanism of PDT effect of $YbPO_4$:Er,Dy-MC540.
Notes: (**A**) Schematic illustration showing how PDT works using $YbPO_4$:Er,Dy-MC540. On exposure to NIR light, the $YbPO_4$:Er,Dy microspheres convert NIR light to visible light, which will activate the MC540 to produce reactive oxygen species to kill cancer cells. (**B**) Overlap between $YbPO_4$:Er,Dy emission and MC540 absorption: upconversion fluorescence spectrum of $YbPO_4$:Er,Dy under NIR laser excitation (red line); ultraviolet–visible absorption spectrum of MC540 in water (blue line).
Abbreviations: MC540, merocyanine 540; NIR, near-infrared; PDT, photodynamic therapy.

microspheres. The inset of Figure 10A shows photographs of MC540, $YbPO_4$:Er,Dy-MC540, and $YbPO_4$:Er,Dy dispersed in PBS under ambient light. Different from typical white-colored non-MC540-loaded $YbPO_4$:Er,Dy dispersion, a clearly lilac color could be seen for $YbPO_4$:Er,Dy-MC540 PBS dispersion, thereby demonstrated successful loading of MC540 onto the $YbPO_4$:Er,Dy. The ultraviolet–visible spectrum with the remarkable absorption-band characteristic of MC540 further identifies the presence of MC540 in the $YbPO_4$:Er,Dy-MC540 sample (blue line in Figure 10A). With help of the calibration curve (Figure S1A), the MC540 concentration in the $YbPO_4$:Er,Dy-MC540 dispersion can be calculated. In contrast, no such peaks could be found in the non-MC540-loaded $YbPO_4$:Er,Dy sample (black line in Figure 10A).

In order to evaluate the in vitro PDT effects of $YbPO_4$:Er,Dy-MC540, HepG2 cells were incubated with $YbPO_4$:Er,Dy-MC540 for 12 hours, and then exposed to 980 nm laser light (0.5 W) for 3 minutes. Satisfactory results of PDT effect were obtained by comparing the cell viabilities of the NIR-light irradiated group ("4" columns in Figure 7) and the non-NIR-light group ("3" columns in Figure 7). As is shown, significant decrease (about 20%–30%) in cell viabilities was observed for all NIR-light irradiated samples even at the low $YbPO_4$:Er,Dy-MC540 concentration of 125 μg/mL.

It is well-known that synergistic effects can be achieved by using different antitumor therapies because they are complementary rather than competitive with each other. In order to achieve an enhanced cancer-cell killing effect, DOX, a widely used chemotherapy drug, was loaded onto the $YbPO_4$:Er,Dy spheres together with MC540 to obtain $YbPO_4$:Er,Dy-MC540-DOX.

Similarly, the loading of DOX onto $YbPO_4$:Er,Dy microspheres was confirmed by the orange color, which is characteristic of DOX, and an ultraviolet–visible spectrum of $YbPO_4$:Er,Dy-DOX dispersion with the remarkable DOX absorption peak at 488 nm (Figure 10B). The DOX amount loaded on the $YbPO_4$:Er,Dy microspheres was also calculated

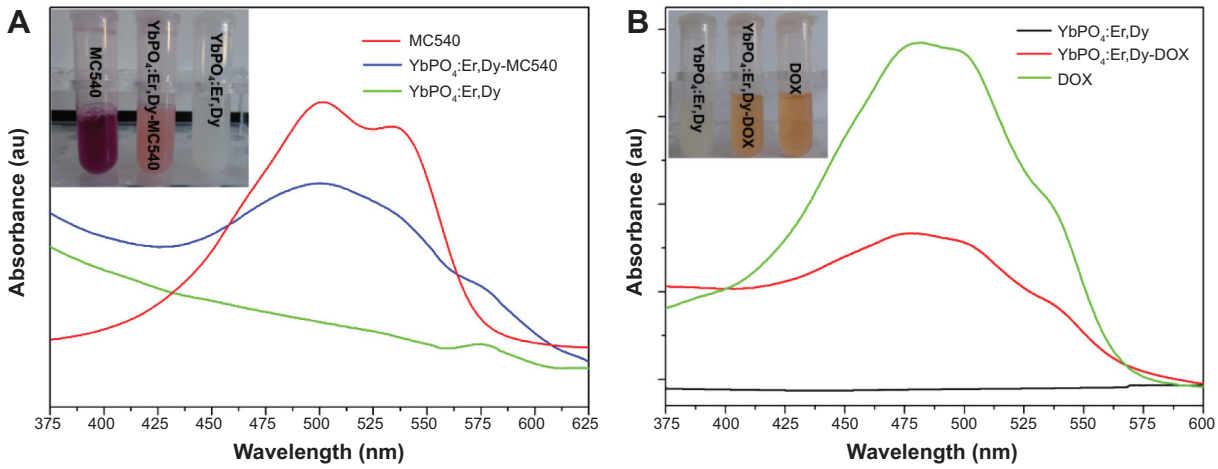

Figure 10 Loading of MC540 and DOX on $YbPO_4$:Er,Dy.
Notes: Ultraviolet–visible absorption spectra of (**A**) MC540, $YbPO_4$:Er,Dy, and $YbPO_4$:Er,Dy-MC540, and (**B**) DOX, $YbPO_4$:Er,Dy, and $YbPO_4$:Er,Dy-DOX PBS dispersion with their digital photos under ambient light shown in the insets.
Abbreviations: DOX, doxorubicin; MC540, merocyanine 540; PBS, phosphate-buffered saline.

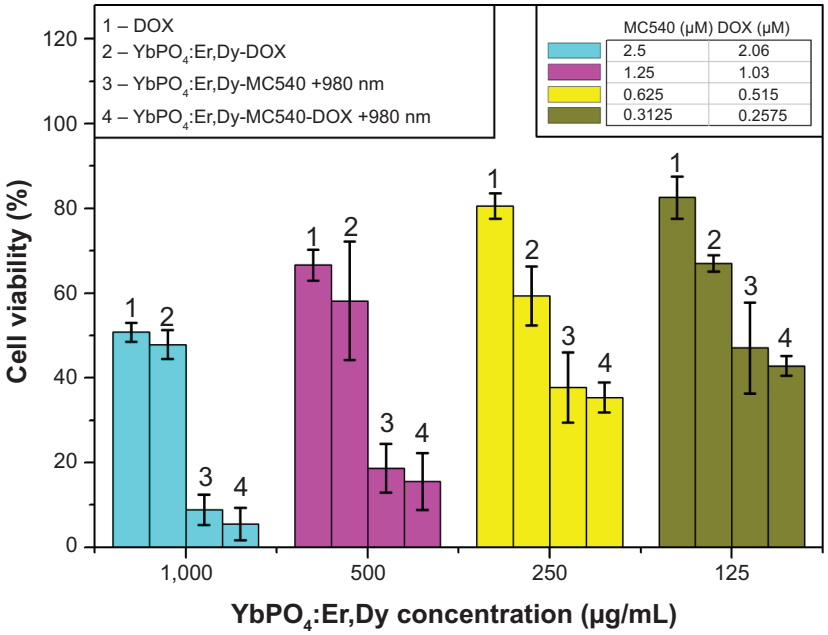

Figure 11 Cell viability data of hepatocellular carcinoma cancer cells showing enhanced antitumor effect of $YbPO_4$:Er,Dy-MC540-DOX.
Notes: Data presented as mean ± standard deviation (n=4). $P<0.05$ when compared with control.
Abbreviations: DOX, doxorubicin; MC540, merocyanine 540.

with help of the calibration curve (Figure S1B). On account of high toxicity of concentrated DOX, we use $YbPO_4$:Er,Dy-MC540-DOX dispersion with DOX concentration not higher than 2.06 μM for further experiments.

The antitumor effect of $YbPO_4$:Er,Dy-MC540-DOX was also assessed by cell viability using an experimental method similar to $YbPO_4$:Er,Dy-MC540. As expected, even larger decreases in cell viabilities were observed for the $YbPO_4$:Er,Dy-MC540-DOX-980 nm group ("4" columns in Figure 11) compared with the $YbPO_4$:Er,Dy-MC540-980 nm ("4" columns in Figure 7 or "3" columns in Figure 11) and $YbPO_4$:Er,Dy-DOX ("2" columns in Figure 11) groups. For example, with the same concentration of $YbPO_4$:Er,Dy of 125 μg/mL, cell viabilities were measured to be 67.00%±1.89% and 47.05%±10.69% for $YbPO_4$:Er,Dy-DOX ("2" green column in Figure 11) and $YbPO_4$:Er,Dy-MC540-980 nm ("3" green column in Figure 11), respectively, but only 42.84%±2.36% for $YbPO_4$:Er,Dy-MC540-DOX-980 nm ("4" green column in Figure 11). This enhanced antitumor efficacy may be ascribed to the synergistic effect of PDT and chemotherapy.

Cytotoxicity of free MC540 and DOX with a series of concentrations was investigated in order to clarify the disturbance-on-cell-viability measurement of these free ligands, which may be produced in the redispersion step of $YbPO_4$:Er,Dy in PBS. As is shown, cell viabilities of free MC540 ("2" columns in Figure 7) and free DOX ("1" columns in Figure 11) are much higher than that of $YbPO_4$:Er,Dy-MC540 ("4" columns in Figure 7) and $YbPO_4$:Er,Dy-MC540-DOX ("4" columns in Figure 11) with equivalent MC540 or DOX loading amounts under 980 nm laser irradiation, indicating low cytotoxicity of free MC540 and DOX in $YbPO_4$:Er,Dy-PBS dispersions.

To differentiate the dead and live cells, TB, which can detect the integrity of the cell membrane, was used to stain the dead cells. As is shown in Figure 12, almost all the cells incubated with $YbPO_4$:Er,Dy-MC540 were stained blue after 980 nm laser excitation, and a distinct boundary of illuminated area can be distinguished from the surrounding

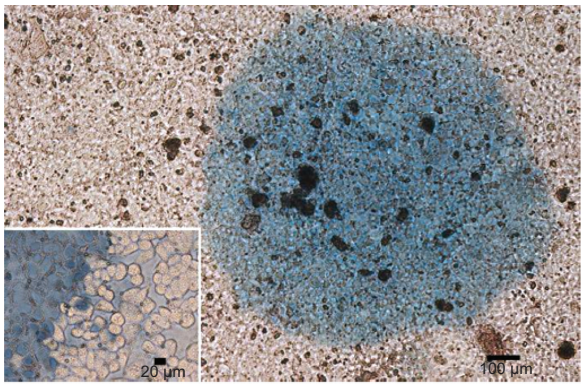

Figure 12 Optical microscopy images of trypan blue stained hepatocellular carcinoma cancer cells incubated with $YbPO_4$:Er,Dy-MC540 for 24 hours and further exposed to 980 nm laser for 3 minutes.
Abbreviation: MC540, merocyanine 540.

area (inset of Figure 12). These results suggest that the death of cells is dominated by the PDT effect of MC540 triggered by the NIR-light irradiated $YbPO_4$:Er,Dy. Due to the deep tissue penetration of NIR light, $YbPO_4$:Er:Dy-MC540 particles possess great potential for in vivo PDT of cancer.

Conclusion

We successfully synthesized upconverting $YbPO_4$:Er,Dy microspheres with uniform morphology by solvothermal method. Sintering temperature and doping ratio greatly influence the fluorescent properties of the products. The samples with stoichiometry of Yb:Er:Dy:PO_4=1.00:0.05:0.05:1.10 sintered at 1,200°C had optimized fluorescence–magnetic bifunctionality, which can enter the HepG2 cells and present low toxicity. By using a well-selected PDT drug of water-soluble MC540, we have succeeded in developing a $YbPO_4$:Er,Dy-based PDT drug, which can kill the HepG2 cells exposed to NIR light effectively. With the assistance of DOX, enhanced antitumor effect was achieved by $YbPO_4$:Er,Dy-MC540-DOX which may be due to synergistic efficacy of PDT and chemotherapy. The combination of visible emission generated by infrared-light excitation, magnetic relaxivity properties, and efficacy of antitumor effect affords the materials great potential in cancer theranostics including bimodal imaging and NIR-light triggered PDT. In spite of desirable fluorescent–magnetic bifunctionality and antitumor effect, the microscale size of our $YbPO_4$:Er,Dy microspheres may hinder their use in clinical settings because particle sizes below 100 nm are generally required in order to avoid: blockage of blood vessels: uptake by macrophages that is too fast; and controlled clearance from the organism. Studies on reducing the size of the $YbPO_4$:Er,Dy spheres are ongoing.

Acknowledgments

This research was financially supported by the Distinguished Middle-Aged and Young Scientist Encourage and Reward Foundation of Shandong Province (Grant BS2012CL015), and Development Program in Science and Technology of Qingdao (Grant 13-1-4-182-jch).

Disclosure

The authors report no conflicts of interest in this work.

References

1. Fang J, Pillai RS, Saunders M, et al. Room temperature synthesis of upconversion fluorescent nanocrystals. *Chem Commun (Camb)*. 2011;47:10043–10045.
2. Hilderbrand SA, Shao F, Salthouse C, Mahmood U, Weissleder R. Upconverting luminescent nanomaterials: application to in vivo bioimaging. *Chem Commun (Camb)*. 2009;(28):4188–4190.
3. Carlos LD, Ferreira RAS, Bermudez Vde Z, Ribeiro SJ. Lanthanide-containing light-emitting organic-inorganic hybrids: A bet on the future. *Adv Mater*. 2009;21:509–534.
4. Wang W, Zou M, Chen KZ. Novel Fe_3O_4@YPO_4:Re (Re = Tb, Eu) multifunctional magnetic-fluorescent hybrid spheres for biomedical applications. *Chem Commun (Camb)*. 2010;46:5100–5102.
5. Macedo AG, Ferreira RAS, Ananias D, et al. Effects of phonon confinement on anomalous thermalization, energy transfer, and upconversion in Ln^{3+}-doped Gd_2O_3 nanotubes. *Adv Funct Mater*. 2010;20:624–634.
6. Debasu ML, Ananias D, Pinho SL, Geraldes CF, Carlos LD, Rocha J. (Gd,Yb,Tb)PO_4 up-conversion nanocrystals for bimodal luminescence-MR imaging. *Nanoscale*. 2012;4:5154–5162.
7. Lee S, Teshima K, Mori S, Endo M, Oishi S. Selective growth of upconverting $YbPO_4$:Ln (Ln = Er or Tm) crystals in a micro reaction cell. *Cryst Growth Des*. 2010;10:1693–1698.
8. Kim WJ, Nyk M, Prasad PN. Color-coded multilayer photopatterned microstructures using lanthanide (III) ion co-doped $NaYF_4$ nanoparticles with upconversion luminescence for possible applications in security. *Nanotechnology*. 2009;20:185301.
9. Suyver JF, Grimm J, Krämer KW, et al. Highly-efficient near-infrared to visible upconversion process in $NaYF_4/Er^{3+}$, Yb^{3+}. *J Lumin*. 2005;114:53–59.
10. Schäfer H, Ptacek P, Eickmeier H, Haase M. Synthesis of hexagonal Yb^{3+},Er^{3+}-doped $NaYF_4$ nanocrystals at low temperature. *Adv Funct Mater*. 2009;19:3091–3097.
11. Wei XJ, Wang W, Chen KZ. Preparation and characterization of ZnS:Tb,Gd and ZnS:Er,Yb,Gd nanoparticles for bimodal magnetic-fluorescent imaging. *Dalton Trans*. 2013;42:1752–1759.
12. Liu Y, Yang Q, Xu C. Single-narrow-band red upconversion fluorescence of ZnO nanocrystals codoped with Er and Yb and its achieving mechanism. *J Appl Phys*. 2008;104:064701.
13. Wei XJ, Wang W, Chen KZ. ZnO:Er,Yb,Gd particles designed for magnetic-fluorescent imaging and near-infrared light triggered photodynamic therapy. *J Phys Chem C*. 2013;117:23716–23729.
14. Nichkova M, Dosev D, Gee SJ, Hammock BD, Kennedy IM. Microarray immunoassay for phenoxybenzoic acid using polymer encapsulated Eu:Gd_2O_3 nanoparticles as fluorescent labels. *Anal Chem*. 2005;77:6864–6873.
15. Nichkova M, Dosev D, Perron R, Gee SJ, Hammock BD, Kennedy IM. Eu^{3+}-doped Gd_2O_3 nanoparticles as reporters for optical detection and visualization of antibodies patterned by microcontact printing. *Anal Bioanal Chem*. 2006;384:631–637.
16. Tan WM, Lu CH, Ni YR, et al. Unique photoluminescence in SiO_2:Sm prepared by sol-gel process. *Chin J Inorg Chem*. 2009;25:635–640.
17. Wang Y, Wu C, Wei J. Hydrothermal synthesis and luminescent properties of $LnPO_4$:Tb,Bi (Ln=La,Gd) phosphors under UV/VUV excitation. *J Lumin*. 2007;126:503–507.
18. Chen G, Sun S, Zhao W, Xu S, You T. Template synthesis and luminescence properties of $CePO_4$:Tb nanotubes. *J Phys Chem C*. 2008;112:20217–20221.
19. de Sousa Filho PC, Serra OA. Reverse microemulsion synthesis, structure, and luminescence of nanosized $REPO_4$:Ln^{3+} (RE = La, Y, Gd, or Yb, and Ln = Eu, Tm, or Er). *J Phys Chem C*. 2011;115:636–646.
20. Yaiphaba N, Ningthoujam RS, Singh NR, Vatsa RK. Luminescence properties of redispersible Tb^{3+}-doped $GdPO_4$ nanoparticles prepared by an ethylene glycol route. *Eur J Inorg Chem*. 2010;18:2682–2687.
21. Liu Y, Ai K, Yuan Q, Lu L. Fluorescence-enhanced gadolinium-doped zinc oxide quantum dots for magnetic resonance and fluorescence imaging. *Biomaterials*. 2011;32:1185–1192.
22. Mulder WJ, Strijkers GJ, van Tilborg GA, Griffioen AW, Nicolay K. Lipid-based nanoparticles for contrast-enhanced MRI and molecular imaging. *NMR Biomed*. 2006;19:142–164.
23. Chatterjee DK, Fong LS, Zhang Y. Nanoparticles in photodynamic therapy: An emerging paradigm. *Adv Drug Delivery Rev*. 2008;60:1627–1637.

24. Bechet D, Couleaud P, Frochot C, Viriot ML, Guillemin F, Barberi-Heyob M. Nanoparticles as vehicles for delivery of photodynamic therapy agents. *Trends Biotechnol*. 2008;26:612–621.
25. Detty MR, Gibson SL, Wagner SJ. Current clinical and preclinical photosensitizers for use in photodynamic therapy. *J Med Chem*. 2004; 47:3897–3915.
26. Lu T, Shao P, Mathew I, Sand A, Sun W. Synthesis and photophysics of benzotexaphyrin: a near-infrared emitter and photosensitizer. *J Am Chem Soc*. 2008;130:15782–15783.
27. Ji HT, Chien LT, Lin YH, Chien HF, Chen CT. 5-ALA mediated photodynamic therapy induces autophagic cell death via AMP-activated protein kinase. *Mol Cancer*. 2010;9:91.
28. Cui S, Chen H, Zhu H, et al. Amphiphilic chitosan modified upconversion nanoparticles for in vivo photodynamic therapy induced by near-infrared light. *J Mater Chem*. 2012;22:4861–4873.
29. Lee SJ, Koo H, Jeong H, et al. Comparative study of photosensitizer loaded and conjugated glycol chitosan nanoparticles for cancer therapy. *J Control Release*. 2011;152:21–29.
30. Shan J, Budijono SJ, Hu G, et al. Pegylated composite nanoparticles containing upconverting phosphors and meso tetraphenyl porphine (TPP) for photodynamic therapy. *Adv Funct Mater*. 2011;21:2488–2495.
31. Li C, Xu Z, Yang D, et al. Well-dispersed KRE_3F_{10} (RE = Sm-Lu, Y) nanocrystals: solvothermal synthesis and luminescence properties. *Cryst Eng Comm*. 2011;14:670–678.
32. Zhang P, Steelant W, Kumar M, Scholfield M. Versatile photosensitizers for photodynamic therapy at infrared excitation. *J Am Chem Soc*. 2007; 129:4526–4527.
33. Chatterjee DK, Yong Z. Upconverting nanoparticles as nanotransducers for photodynamic therapy in cancer cells. *Nanomedicine (Lond)*. 2008; 3:73–82.
34. Wang C, Cheng L, Liu Y, et al. Imaging-guided pH-sensitive photodynamic therapy using charge reversible upconversion nanoparticles under near-infrared light. *Adv Funct Mater*. 2013;23:3077–3086.
35. Wang M, Chen Z, Zheng W, et al. Lanthanide-doped upconversion nanoparticles electrostatically coupled with photosensitizers for near-infrared-triggered photodynamic therapy. *Nanoscale*. 2014;6:8274–8282.
36. Park YII, Kim HM, Kim JH, et al. Theranostic probe based on lanthanide-doped nanoparticles for simultaneous in vivo dualmodal imaging and photodynamic therapy. *Adv Mater*. 2012;24:5755–5761.
37. Qiao XF, Zhou JC, Xiao JW, et al. Triple-functional core-shell structured upconversion luminescent nanoparticles covalently grafted with photosensitizer for luminescent, magnetic resonance imaging and photodynamic therapy in vitro. *Nanoscale*. 2012;4:4611–4623.
38. Zeng LY, Xiang LC, Ren WZ, et al. Multifunctional photosensitizer-conjugated core-shell Fe_3O_4@$NaYF_4$:Yb/Er nanocomplexes and their applications in T_2-weighted magnetic resonance/upconversion luminescence imaging and photodynamic therapy of cancer cells. *RSC Adv*. 2013;3:13915–13925.
39. Guo H, Qian H, Idris NM, Zhang Y. Singlet oxygen-induced apoptosis of cancer cells using upconversion fluorescent nanoparticles as a carrier of photosensitizer. *Nanomedicine.* 2010;6:486–495.
40. Idris NM, Gnanasammandhan MK, Zhang J, Ho PC, Mahendran R, Zhang Y. In vivo photodynamic therapy using upconversion nanoparticles as remote-controlled nanotransducers. *Nat Med*. 2012;18: 1580–1585.
41. Das GK, Johnson NJJ, Cramen J, et al. $NaDyF_4$ nanoparticles as T_2 contrast agents for ultrahigh field magnetic resonance imaging. *J Phys Chem Lett*. 2012;3:524–529.
42. Soesbe TC, Ratnakar JS, Kovacs Z, et al. Using T_2-exchange from Dy^{3+} DOTA-based chelates for contrast-enhanced molecular imaging with MRI[C]. Proceedings of the 21st Annual Meeting of ISMRM, Salt Lake City, Utah, USA. 20–26 April, 2013.
43. Ren G, Zeng S, Hao J. Tunable multicolor upconversion emissions and paramagnetic property of monodispersed bifunctional lanthanide-doped $NaGdF_4$ nanorods. *J Phys Chem C*. 2011;115:20141–20147.
44. Wang L, Li Y. Controlled synthesis and luminescence of lanthanide doped $NaYF_4$ nanocrystals. *Chem Mater*. 2007;19:727–734.
45. Matsuura D. Red, green, and blue upconversion luminescence of trivalent-rare-earth ion-doped Y_2O_3 nanocrystals. *Appl Phys Lett*. 2002; 81:4526–4528.
46. Jordan FL, Wynder HJ, Booth PL, Thomas WE. Method for the identification of brain macrophages/phagocytic cells in vitro. *J Neurosci Res*. 1990;26:74–82.
47. Stringer B, Imrich A, Kobzik L. Flow cytometric assay of lung macrophage uptake of environmental particulates. *Cytometry*. 1995;20: 23–32.
48. Wei W, Wang L-Y, Yuan L, et al. Preparation and application of novel microspheres possessing autofluorescent properties. *Adv Func Mater*. 2007;17:3153–3158.

Supplementary materials

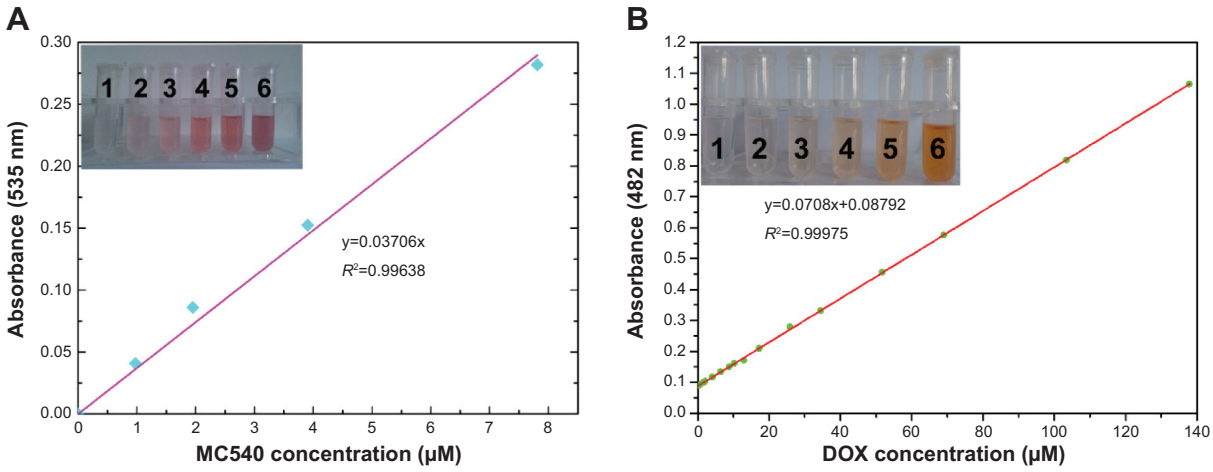

Figure S1 Calibration curves.
Notes: (**A**) MC540 and (**B**) DOX in PBS.
Abbreviations: DOX, doxorubicin; MC540, merocyanine 540; PBS, phosphate-buffered saline.

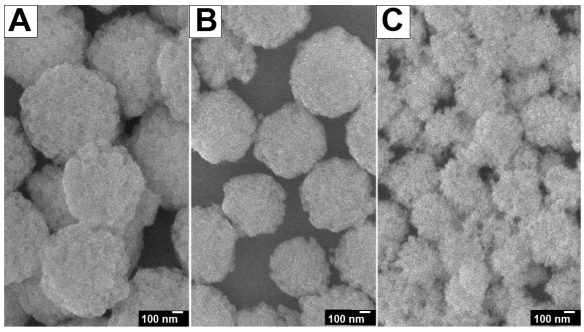

Figure S2 Scanning electron microscope images of YbPO$_4$:Er,Dy microspheres.
Notes: (**A**) Desiccation at 200°C; (**B**) after 800°C sintering; (**C**) after 1,200°C sintering.

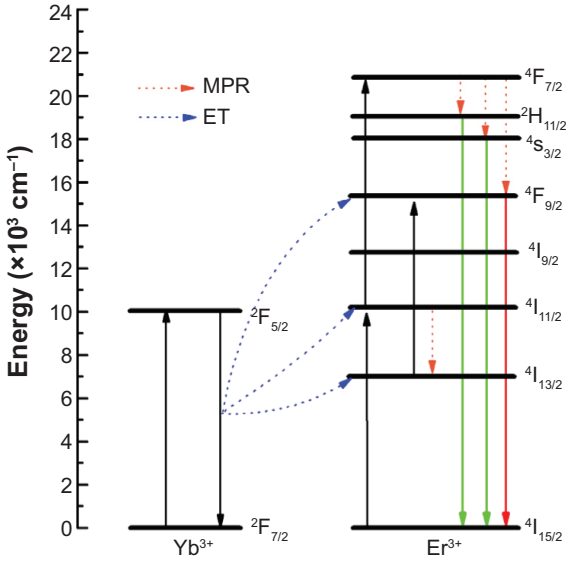

Figure S3 Schematic energy-level diagrams of the Yb^{3+} and Er^{3+} ions in YbPO$_4$:Er and the upconversion mechanism excited by a 980 nm diode laser.
Abbreviations: ET, energy transfer; MPR, multiphonon relaxation.